Mn-doped $CuGaS_2$ chalcopyrites: An *ab initio* study of ferromagnetic semiconductors

Silvia Picozzi
Istituto Nazionale di Fisica della Materia (INFM) and Dipartimento di Fisica, Università degli Studi di L'Aquila, 67010 Coppito (L'Aquila), Italy

Yu-Jun Zhao and Arthur J. Freeman
Department of Physics and Astronomy and Materials Research Center, Northwestern University, Evanston, Illinois 60208

Bernard Delley
Paul Scherrer Institut, WHGA/123 CH-5232 Villigen PSI, Switzerland
(Received 3 July 2002; published 20 November 2002)

Stimulated by our recent findings suggesting that the I-III-VI_2 chalcopyrites could be a different class of ferromagnetic semiconductors, we performed first-principles calculations within density-functional theory and the generalized gradient approximation for Mn-doped $CuGaS_2$. Our calculations confirm the previous theoretical predictions on $CuGaSe_2$, that the ferromagnetic spin configuration is strongly favored. Mn is found to be, as expected, both a source of localized magnetic moments and an acceptor; thus, our results seem to support the general idea that ferromagnetism is stabilized through a carrier-mediated interaction. For all the systems, we find a half-metallic character, consistent with the integer value of the total magnetic moment of $4\mu_B$ per Mn atom. This is particularly important for spin-injection applications: in a significant energy range (i.e., about 0.5 eV in the dilute case) around the Fermi level relevant for spin injection, the holes will have a well-defined spin. A simple Heisenberg model to estimate the Curie temperature T_c in ordered $CuMn_xGa_{1-x}S_2$ alloys gives $T_c \sim 160$ K, therefore suggesting the possible importance of this class of ferromagnetic semiconductors for spintronic applications.

DOI: 10.1103/PhysRevB.66.205206 PACS number(s): 75.50.Pp, 71.20.−b, 75.30.Hx

I. INTRODUCTION

The new discipline called ''spintronics[1]'' which aims at using the spin of electrons (rather than their charge) for storing and processing quantum information, has recently raised a great deal of interest in spin-related phenomena in semiconductors. The dilute magnetic semiconductors (DMS) are semiconductor compounds in which a fraction of the constituent atoms is replaced by magnetic ions. In particular, DMS with the desired magnetic properties, i.e., ferromagnetism, have so far been confined to molecular-beam-epitaxy-grown materials, such as Mn-doped III-V (InMnAs and GaMnAs with Curie temperatures up to 110 K, the focus of both experimental[1] and theoretical[2–5] interests) and II-VI [*p*-doped CdMnTe quantum wells and ZnMnTe epilayers, with extremely low (<3 K) Curie temperatures] materials.[6] It has been shown theoretically[7] that the ferromagnetic (FM) alignment has to be ascribed to a carrier-mediated interaction or Zener model, in which antiferromagnetic (AFM) exchange coupling partially spin polarizes the holes present in the system, which in turn cause an alignment of the local Mn spins. Moreover, semiphenomenological models have been developed, in which the low-energy degrees of freedom are exchange-coupled valence-band holes and $S=5/2$ Mn local moments.[8]

Currently, there is an urgent need to find new materials showing room-temperature ferromagnetism which could open the way to the practical realization of commercial spin-based solid-state devices. Within this framework, we point out the important class of II-GeP_2 (II=Cd, Zn) chalcopyrite systems, where room-temperature ferromagnetism was experimentally reported by Medvedkin *et al.* in Mn-doped $CdGeP_2$ (Ref. 9) and more recently by Cho *et al.* in Mn-doped $ZnGeP_2$.[10] It was subsequently shown by theoretical calculations[11,12] that the AFM alignment is the ground state at $T=0$ of all the Mn-doped II-Ge-V_2 (II=Cd, Zn and V=P, As) compounds. Moreover, it was pointed out in Ref. 13 that, for Mn-doped $CdGeP_2$, in the absence of intrinsic defects, the Mn-Cd substitution is favored in a large range of growth conditions. However, chalcopyrites exhibit low-energy intrinsic defects; therefore, Mahadevan and Zunger[13] showed that, depending on the growth conditions, Mn can even substitute Ge and the interaction between Mn and hole-producing defects could stabilize FM. The theoretically predicted AFM ground state at T=0 in this class of systems is consistent with the experimental observation[10] that $Zn_{1-x}Mn_xGeP_2$ experiences a FM-to-AFM transition below 47 K. However, an understanding of this unusual magnetic phase transition and of ferromagnetism without carriers in this class of materials is still unclear and so more experimental and theoretical work is called for.

In a recent paper,[14] we predicted a class of ferromagnetic semiconductors, represented by I-III-VI_2 (I=Cu, Ag; III=Al, Ga, In; and VI=S, Se, Te) chalcopyrite ternary compounds doped with Mn. In particular, *ab initio* calculations [using both the full-potential linearized augmented plane-wave (FLAPW) (Ref. 15) and density-functional theory for molecules and three-dimensional periodic solids (DMol^3) methods)] (Ref. 16) were performed for $CuGaSe_2$, Mn was found to substitute preferentially for Ga rather than for Cu and the ferromagnetic state was strongly favored, with a predicted Curie temperature of 100–150 K. It was suggested

that while still too low for applications, this finding could open the way to other I-III-VI_2 compounds with higher Curie temperatures.

Within this same framework, we performed first-principles calculations on chalcopyrite $CuGaS_2$ doped with Mn, focusing on different aspects: (i) Mn point defects in $CuGaS_2$, in terms of formation energies and impurity states in the gap; (ii) The structural, electronic, and magnetic properties of the $CuMn_xGa_{1-x}S_2$ ordered alloys as a function of the Mn concentration and comparisons to the $CuMn_xGa_{1-x}Se_2$ system.

II. COMPUTATIONAL DETAILS

Both the DMol^3 (Ref. 16) and FLAPW (Ref. 15) methods are used. The DMol^3 method was recently successfully applied to other magnetic semiconductors.[2] The localized numerical orbitals, used as basis set, are designed to give a high level of accuracy; DMol^3 relies fully on the efficient three-dimensional numerical integrations of the matrix elements occurring in the Ritz variational method. Scalar relativistic effects via a local pseudopotential for all-electron calculations are included in the method.[17] In the present work, we employ a double set of numerical valence functions with a local basis cutoff R_c of 9.0 a.u. The structural degrees of freedom (internal relaxations and lattice constants, where not available from experiments) are optimized using DMol^3, and the final equilibrium geometry is checked using the highly precise FLAPW method.

In the all-electron self-consistent FLAPW method,[15] the core electrons are treated fully relativistically, whereas scalar-relativistic effects are considered for the valence electrons. Angular momenta up to $l_{max}=8$ in the muffin-tin (MT) spheres and plane waves with wave vectors up to $k_{max}=3.0$ a.u. are used in the wave-function expansion. The muffin-tin radii are chosen as $R_{MT}(\mathrm{Ga})=R_{MT}(\mathrm{Cu})=2.4$ a.u., $R_{MT}(\mathrm{Mn})=2.3$ a.u., and $R_{MT}(\mathrm{S})=1.9$ a.u. To perform integrations in reciprocal space, we use both the special **k**-points method (a set of 4–24 special **k** points is chosen in the irreducible Brillouin zone, following the Monkhorst-Pack scheme[18]) and the tetrahedron method.[19]

In both the DMol^3 and FLAPW calculations, we use the generalized gradient approximation (GGA) to the exchange-correlation potential in the density-functional theory framework, according to the Perdew-Becke-Erzenhof scheme.[20]

III. STRUCTURAL DETAILS

A. Defect calculations

The defect calculations are performed by placing a single Mn atom in a large orthorhombic unit cell, containing 32 atoms and having lattice vectors $(2,0,0)a$, $(0,1,0)a$, and $(0,0,\eta)a$; the lattice parameters a and $c=2a\,\eta$ are chosen as for the pure bulk chalcopyrites and the internal degrees of freedom are optimized by minimizing the *ab initio* DMol^3 forces, so as to yield the equilibrium geometry around the Mn defect. This system is an intermediate case between the ideally isolated impurity in $CuGaS_2$ and the ordered alloys (see below). In this particular type of defect calculations, due to the choice of the unit cell with a single Mn atom, the systems are in a ferromagnetic configuration. We consider substitutional defects, i.e., replacing a single cation (namely Cu and Ga) with a Mn atom in the pure chalcopyrite $CuGaS_2$ cell. Here, we do not consider interstitial or charged defects.

The formation energy of a defect α is estimated as follows.[21]

$$\Delta H_f(\alpha)=\Delta E(\alpha)+n_{Cu}\mu_{Cu}+n_{Ga}\mu_{Ga}+n_{Mn}\mu_{Mn}, \quad (1)$$

where

$$\Delta E(\alpha)=E(\alpha)-E^{ch}+n_{Cu}\mu^0_{Cu}+n_{Ga}\mu^0_{Ga}+n_{Mn}\mu^0_{Mn}. \quad (2)$$

$E(\alpha)$ and E^{ch} are the total energies of the unit cell with and without the defect, respectively. μ_i denotes the chemical potential and takes into account, in forming a defect, that the atom is transferred to or from a chemical reservoir that has a characteristic energy, μ_i. The chemical potential of constituent i can be expressed with respect to its chemical potential in its stable phase μ_i^0, so that $\mu_i=\mu_i^a+\mu_i^0$ (a denotes the absolute value). The stable phases are calculated at the equilibrium lattice constant for AFM Mn (Ref. 22), α-Ga (Ref. 23), and fcc Cu.[24] The n_i are the number of atoms transferred from the supercell to the reservoir in forming the defect. We consider the particular thermodynamic limit $\mu_i=0$, so that we obtain $\Delta H_f=\Delta E(\alpha)$.

The calculations of the pure unit cell (i.e., no impurity present) are performed using the same unit cell as well as the same computational parameters (e.g., **k**-point sampling, wave function cutoffs) as in the case of the Mn defect cell. We estimate an overall uncertainty of about 0.2 eV in the defect formation energy, arising from the unphysical defect-defect interaction of our 32-atom cell, and the numerical uncertainty within GGA in calculating the heats of formation and the computational parameters.

B. Ordered alloys

In order to simulate systems with a large concentration of Mn, we consider some $CuMn_xGa_{1-x}S_2$ systems, for $x=0.125$, 0.25, 0.5, and 1.0. In particular, we consider Mn substituting for the type-III atom in the original chalcopyrite structure (see below). Since experimental data are not available for $CuMnS_2$ (i.e., $x=1$), its lattice parameters have been optimized using DMol^3, yielding $a=5.39$ Å and $c=2a\,\eta=10.57$ Å (or, equivalently, $\eta=0.98$). On the other hand, those for bulk chalcopyrites have been taken from the experiments.[25] for $CuGaS_2$, $a=5.35$ Å and $c/2a=0.98$. For the intermediate concentrations, we consider a linear interpolation between those of pure $CuGaS_2$ and $CuMnS_2$ chalcopyrites, assuming Vegard's law. In order to study the favored magnetic alignment, we consider some "spin superlattices" with period p and ordering direction **G**(**G**$=[001]$ for $x=1.0$, 0.5—denoted as AFM(I)—and **G**$=[100]$ for $x=0.125$, 0.25, 0.5—denoted as AFM(II)). As pointed out in Ref. 14, the paramagnetic state does not compete with the FM or AFM alignments, since, for example, the DMol^3 calculated total energy of the paramagnetic state in a similar

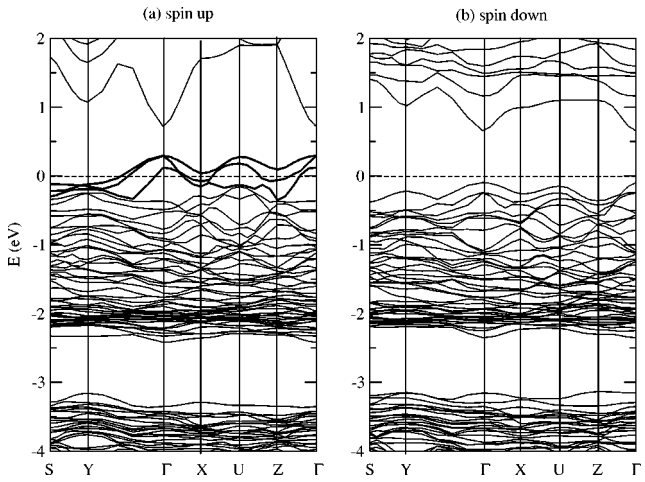

FIG. 1. (a) Spin-up and (b) spin-down band structures for the Mn defect in $CuGaS_2$ along the main symmetry directions in the Brillouin zone.

compound, $CuGa_{0.75}Mn_{0.25}Se_2$, is about 240 meV higher than the corresponding ferromagnetic configuration.

IV. FORMATION ENERGY OF POINT DEFECTS AT SMALL MN CONCENTRATIONS

The formation energies of a Mn defect in $CuGaS_2$ are calculated to be $\Delta E(\mathrm{Mn}_{Ga}) = 0.43$ eV and $\Delta E(\mathrm{Mn}_{Cu}) = 0.80$ eV for Mn substituting Ga and Cu, respectively. In the chosen limit of the chemical potentials, this implies that the substitution of a group III atom (rather than Cu) by Mn is strongly favored. The formation energies are similar to those obtained for $CuGaSe_2$, where $\Delta E(\mathrm{Mn}_{Ga}) = 0.48$ eV and $\Delta E(\mathrm{Mn}_{Cu}) = 0.73$ eV. The formation energies of a Mn defect in Cu-III-VI_2 chalcopyrites is of the same order of magnitude as in GaAs [$\Delta E(\mathrm{Mn}_{Ga}) = 0.52$ meV/Mn]; a massive doping of Mn in chalcopyrites could therefore be inhibited by the limited solubility (i.e., the largest concentration of Mn achieved in GaAs, without clustering, is about 7%).

As a consequence, since the 2^+ Mn preferentially goes into the 3^+ site, we expect defect bands providing holes to occur. This is actually found from our calculations: the typical acceptor nature of Mn is clearly shown in Fig. 1, where we plot the band structure of Mn in $CuGaS_2$. Due to the finite Mn concentration, impurity bands arise; the defect bands (thicker lines) around the Fermi level in the spin-up band structure have a width of ~ 0.5 eV. This quite broad feature is a signature of hybridization and has to be ascribed mainly to Mn $3d$ and S $3p$ states. On the other hand, a clear semiconducting character is shown by the spin-down band structure, since the Fermi level cuts a 1-eV band gap. As a result, the system is half metallic, i.e., a spin band is completely empty at E_F. This is particularly useful in view of spin-injection applications; holes in proximity to E_F, i.e., the relevant energy range for injection, will have a well-defined spin. A closer inspection of the band structure shows that, in the majority-spin channel, a band gap also arises in the [0.3–0.75] eV energy range; both the band gaps in the majority- and minority-spin states are direct (as in the $CuGaS_2$ host crystal), but, due to the Mn concentration, the valence-band maximum (VBM) in the minority bands is lower by about 0.4 eV compared to the majority VBM.

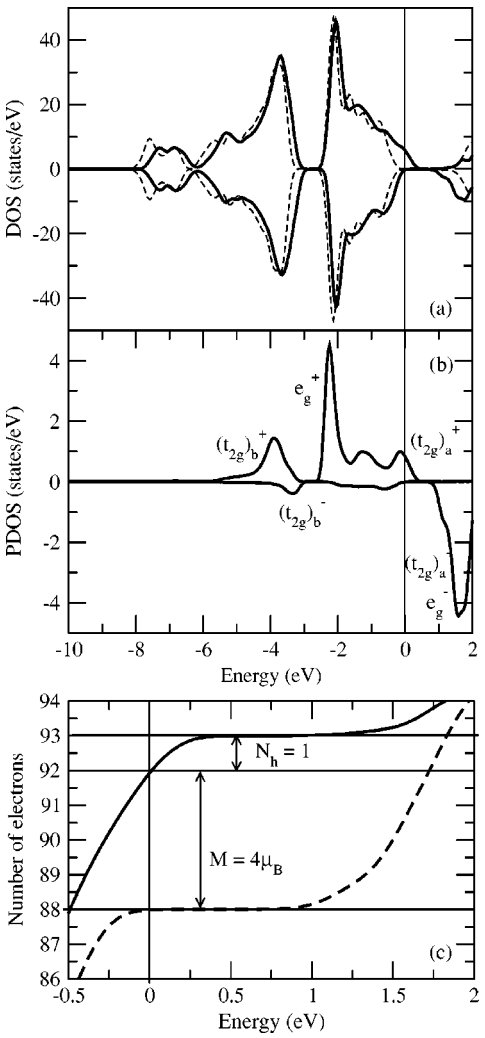

FIG. 2. (a) Total density of states for the Mn defect in $CuGaS_2$ (solid) and for the pure bulk chalcopyrite $CuGaS_2$ (dashed). (b) Projected Mn $3d$ density of states. (c) Integrated density of states for up-spin (solid) and down-spin (dashed) channels.

Further insights can be gained from (i) the total density of states (DOS) of the Mn defect in $CuGaS_2$ [Fig. 2(a)], compared to that of pure bulk semiconducting $CuGaS_2$ and (ii) from the DOS [Fig. 2(b)] projected on the Mn atom (only $3d$ states are shown, since $4s$ states give negligible contributions). As shown in Fig. 2(a), the perturbation introduced by the magnetic Mn atom is mainly evident in the energy range from -1 eV up to 2 eV; as expected, its effect on the host DOS is an exchange splitting of the valence band and, due to hybridization, a reduction of the band gaps in both the majority- and the minority-spin channels. Moreover, as pointed out in Ref. 26, the Ga-substitutional site has a local tetrahedral symmetry, so that the higher-lying Mn $3dt_{2g}$ (xy,yz, and xz) orbitals strongly interact with the nearest-neighbor tetrahedrally coordinated S atoms. As a result, bonding [$(t_{2g})_b$] and antibonding [$(t_{2g})_a$] states form [see Fig. 2(b)], with $(t_{2g})_b$ located well inside the valence band

TABLE I. FLAPW calculated magnetic properties of $CuMn_xGa_{1-x}S_2$ as a function of Mn concentration x.

	$CuMn_{0.25}Ga_{0.75}S_2$		$CuMn_{0.5}Ga_{0.5}S_2$		$CuMnS_2$	
	FM	AFM	FM	AFM	FM	AFM
Total energy (meV/Mn)	0	53	0	89	0	105
Total magnetic moment (μ_B/Mn)	4	0	4	0	4	0
Mn magnetic moment (μ_B)	3.77	± 3.80	3.78	± 3.77	3.76	± 3.4

and $(t_{2g})_a$ pushed up in energy; in particular, in the spin-up DOS, $(t_{2g})_b$ lies in the $CuGaS_2$ band gap. On the other hand, the Mn $3d$ e_g orbitals ($3z^2-r^2$ and x^2-y^2) are basically unaffected by the presence of the host crystal, forming well-localized nonbonding states. As a result, the PDOS on the Mn atom shows a spin-up (-down) contribution that is mostly occupied (unoccupied), leading to a magnetic moment, (mainly of Mn $3d$ origin), of 3.81 μ_B in the Mn MT sphere and a total magnetic moment of $4\mu_B$. The integer value of the total magnetic value is consistent with the marked half-metallic behavior shown in the band structure (Fig. 1) and in the total DOS [Fig. 2(a)].

The integrated density of states (IDOS) is plotted in Fig. 2(c), i.e., for every energy E the number of states with energy less than E, for the majority-and minority-spin channels. It is evident that, consistent with that reported in Ref. 27 for many IV, III-V, and N-doped II-VI ferromagnetic DMS, (i) the number of valence minority-spin electrons is not changed by the Mn impurity (i.e., from the IDOS, we obtain, at E_F, half of the total number of valence electrons in a pure $CuGaS_2$ 32-atoms cell) and (ii) each Mn impurity adds five additional majority-spin states to the valence band. Now, since Mn (Ga) has 7 (3) valence electrons, there will only be a net of four electrons contributed by each Mn substituting Ga to fill the majority-spin band. As a result, we expect (and indeed find from the IDOS) that every Mn impurity adds a single hole carrier ($N_h=1$) to the otherwise perfect $CuGaS_2$ crystal and the total magnetic moment amounts to $4\mu_B$.

As a last remark, we note that the Mn atom induces small negative moments (about $-0.06\mu_B$) on both the nearest-neighbor S atoms and second-nearest-neighbor Cu atoms. The negative-anion polarization is believed to be a signature of the AFM coupling between the polarized hole and the Mn spin in the Zener model[7] that was proposed to explain DMS ferromagnetism.

V. FORMATION OF ORDERED ALLOYS AT LARGE MN CONCENTRATIONS

The FLAPW calculated relevant properties of $CuMn_xGa_{1-x}S_2$ are reported in Table I, as a function of the Mn concentration x, for the FM and AFM configurations. For every concentration, the lower total energy of the FM state (set to zero) compared to the AFM state shows that the introduction of Mn in $CuGaS_2$ results in a very stable ferromagnetic semiconductor. The difference between the AFM and FM total energies (Δ_{FA}) increases with Mn concentration.

In Fig. 3(a), we plot the total DOS for the $x=0.5$ case for the FM (solid) and AFM (dashed) systems; we show the DOS projected on the Mn and nearest-neighbor S atoms in Figs. 3(b) and 3(c), respectively. As already pointed out for the defect calculations, $CuMn_{0.5}Ga_{0.5}S_2$ shows a marked half-metallic behavior in proximity to the E_F, whereas the AFM alignment is clearly metallic. A comparison between Fig. 3(b) and 3(c) confirms the bonding, antibonding, and nonbonding features already pointed out in the preceding section for the dilute impurity limit. Let us define the crystal-field splitting Δ_{CF} (exchange splitting Δ_x) as the energy difference between t_{2g} and e_g (e_g^+ and e_g^-) states. In our case, $\Delta_{CF}<\Delta_x$, and the half-metallic high-spin ground state is stabilized, with the $+$ $(-)$ spin state being metallic (semiconductor).

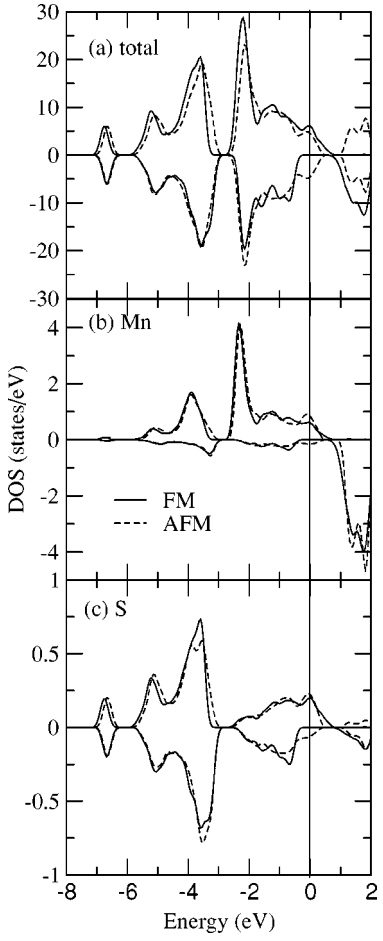

FIG. 3. Density of states for the FM (solid) and AFM (dashed) $CuMn_{0.5}Ga_{0.5}S_2$ system: (a) total, (b) Mn, and (c) nearest-neighbor S PDOS, where positive (negative) values are for spin-up (-down).

According to the generalized double-exchange ferromagnetic interaction,[28] the presence of itinerant holes in the partially occupied $(t_{2g})_a$ bands lowers the band energy, therefore stabilizing the ferromagnetic phase. Our calculations seem to be consistent with this model. It was also argued[2] that in magnetic semiconductors, the antiferromagnetic interaction between Mn $3d$ and its nearest-neighbor anion p states could lower the total energy, therefore stabilizing the ferromagnetic alignment. This is also the case in the system investigated here: as pointed out for the defect cell, the magnetic moment induced by the presence of Mn on the nearest-neighbor S atom is slightly negative (about $-0.01\mu_B$) and the ferromagnetic alignment is strongly favored. Note also that, consistent with previous calculations, the Mn-S bond length in the FM case is slightly shorter than in the AFM case (2.327 Å vs 2.336 Å), resulting in a stronger magnetic interaction. As a final remark, note that the small difference between the Mn $3d$ PDOS in FM and AFM, consistent with the similar magnetic moments, suggests that the moments for $x \leqslant 0.5$ are weakly coupled.

As for a comparison between $CuMnGaS_2$ and $CuMnGaSe_2$,[14] we note that the electronic and magnetic properties (in terms of half metallicity and magnetic moments) are very similar. For $CuMn_xGa_{1-x}Se_2$, the FLAPW calculated Δ_{FA} are 134, 71, and 56 meV at $x=1.0$, 0.5, and 0.25, respectively, resulting in a Δ_{FA} trend vs Mn concentration that is similar to $CuMn_xGa_{1-x}S_2$. According to the hole-mediated ferromagnetic model proposed by Dietl *et al.*,[7] the Curie temperature is proportional to the concentration of cation sites and therefore should be higher for crystals with smaller lattice constants (recall that the experimental lattice constants for $CuGaSe_2$ are $a=5.596$ Å and $c/a=0.98$). Therefore, in order to evaluate the Heisenberg exchange constants J_n (exchange-interaction energy between the nth nearest neighbors) and the Curie temperature T_c, we follow the same procedure used previously in Ref. 14 for $CuMn_xGa_{1-x}Se_2$.

According to a Heisenberg Hamiltonian, we express the difference between the FM and AFM configurations for Mn concentration x in terms of the exchange constants as $\Delta_{FA}=\Sigma\alpha_n J_n(x)$. Using the empirical power-law dependence of J_n on distance,[29] $J_n \propto R_n^{-\lambda}$, we get $\lambda \sim -6$ for the $x=0.5$ case; this is also used for $x=0.25$. In Table II, we show the Dmol^3 calculated Δ_{FA}, along with the expression of this same quantity in terms of the x dependent exchange constants. The J_1 values inferred from Table II are 34.8 meV, 33.9 meV, and 19.2 meV for $x=0.5$, 0.25, and 0.125, respectively. The optimum way to estimate the Curie temperature from the exchange constants is still a matter of debate; however, recalling the similarity of zinc blende and chalcopyrite crystal structures and employing the results of a Monte Carlo simulation[30] for the zinc-blende-based $Cd_{1-x}Mn_xTe$ compound, i.e., $T_c=0.447|J_1|$, we get 180 K, 176 K, and 100 K for $x=0.5$, 0.25, and 0.125, respectively. The comparison with $CuMn_xGa_{1-x}Se_2$, where the estimated Curie temperature was 142 K and 114 K for $x=0.5$, and $x=0.25$, respectively ($x=0.125$ was not considered in Ref. 14), shows the expected tendency for the smaller crystal to have a higher T_c; for example, in going from $CuMn_{0.5}Ga_{0.5}Se_2$ to $CuMn_{0.5}Ga_{0.5}S_2$, an increase of 24% in T_c corresponds to a decrease of 14% in the volume.

TABLE II. Dmol^3 calculated total-energy difference (Δ_{FA}, in meV/Mn) between the ferromagnetic and antiferromagnetic spin states as a function of the Mn concentration x in $CuMn_xGa_{1-x}S_2$ for different ordering directions **G** and period p of spin superlattices. N denotes the number of atoms in the unit cell.

x	p	**G**	N	Δ_{FA}	$\Sigma\alpha_n J_n(x)$
0.5 AFM(I)	1	[001]	16	89.4	$8J_2$
0.5 AFM(II)	2	[100]	32	87.0	$2J_1+4J_3$
0.25	1	[100]	32	84.8	$2J_1+4J_2$
0.125	1	[100]	64	76.8	$4J_1$

VI. CONCLUSIONS

First-principles FLAPW and DMol^3 calculations were performed for $CuMn_xGa_{1-x}S_2$, as a function of the Mn concentration ($x=0.125$, 0.25, 0.5, and 1.0). Our results show that the substitution of Ga by Mn stabilizes the ferromagnetic phase, in agreement with what was predicted in Ref. 14 for the similar $CuMn_xGa_{1-x}Se_2$ compound. Mn is shown to be a source of spins and holes at the same time, so that a mechanism similar to Mn in GaAs is believed to occur here—thus supporting the general idea of ferromagnetism stabilized by a carrier-mediated interaction. In particular, for the dilute case, the presence of a spin-split valence-band edge and a Fermi level cutting the valence band (band gap) in the majority- (minority-) spin states results in half metallicity. As a result, in proximity to E_F, i.e., in the energy range relevant for spin injection, holes will have a well-defined spin. Moreover, half-metallic properties are obtained for all Mn concentrations, with a total magnetic moment of $4\mu_b$ per Mn atom. The commonly employed Heisenberg Hamiltonian was used to estimate the Curie temperature, resulting in $T_c \sim 180$ K and 176 K for $x=0.5$ and $x=0.25$, respectively, higher than the previously studied $CuMn_xGa_{1-x}Se_2$ case.

ACKNOWLEDGMENTS

Work at Northwestern University was supported by DARPA.

[1] H. Ohno, Science **281**, 951 (1998); Y. Ohno, D.K. Young, B. Beschoten, F. Matsukura, H. Ohno, and D.D. Awschalom, Nature (London) **402**, 790 (1999).

[2] Y.J. Zhao, W.T. Geng, K.T. Park, and A.J. Freeman, Phys. Rev. B **64**, 035207 (2001).

[3] S. Sanvito and N.A. Hill, Appl. Phys. Lett. **78**, 3493 (2001); S. Sanvito, P. Ordejon, and N.A. Hill, Phys. Rev. B **63**, 165206 (2001), and references therein.

[4] M. Jain, L. Kronik, J.R. Chelikowski, and V.V. Godlevsky, Phys. Rev. B **64**, 245205 (2001).
[5] M. van Schilfgaarde and O.N. Mryasov, Phys. Rev. B **63**, 233205 (2001).
[6] A. Haury, A. Wasiela, A. Arnoult, J. Cibert, S. Tatarenko, T. Dietl, and Y. Merlè d'Aubigné, Phys. Rev. Lett. **79**, 511 (1997); D. Ferrand, J. Cibert, C. Bourgognon, S. Tatarenko, A. Wasiela, G. Fishman, A. Bonanni, H. Sitter, S. Kolesnik, J. Jaroszyski, A. Barcz, and T. Dietl, J. Cryst. Growth **214/215**, 387 (2000).
[7] T. Dietl, H. Ohno, F. Matsukura, J. Cibert, and D. Ferrand, Science **287**, 1019 (2000).
[8] J. König, T. Schliemann, T. Jungwirth, and A. H. Mac Donald, in *Electronic Structure and Magnetism of Complex Materials*, edited by D. J. Singh and D. A. Papaconstantopoulos (Springer Verlag, Berlin, 2002), and references therein.
[9] G.A. Medvedkin, T. Ishibashi, T. Nishi, K. Hayata, Y. Hasegawa, and K. Sato, Jpn. J. Appl. Phys., Part 2 **39**, L949 (2000).
[10] S. Cho, S. Choi, G.-B. Cha, S.C. Hong, Y. Kim, Y.-J. Zhao, A.J. Freeman, J.B. Ketterson, B.J. Kim, Y.C. Kim, and B.-C. Choi, Phys. Rev. Lett. **88**, 257203 (2002).
[11] Y.-J. Zhao, W.T. Geng, A.J. Freeman, and T. Oguchi, Phys. Rev. B **63**, R201202 (2001).
[12] Y.-J. Zhao, S. Picozzi, A. Continenza, W.T. Geng, and A.J. Freeman, Phys. Rev. B **65**, 094415 (2002).
[13] P. Mahadevan and A. Zunger, Phys. Rev. Lett. **88**, 047205 (2002).
[14] Y.-J. Zhao and A.J. Freeman, J. Magn. Magn. Mater. **246/1-2**, 145 (2002).
[15] E. Wimmer, H. Krakauer, M. Weinert, and A.J. Freeman, Phys. Rev. B **24**, 864 (1981); H.J.F. Jansen and A.J. Freeman, *ibid.* **30**, 561 (1984).
[16] B. Delley, J. Chem. Phys. **113**, 7756 (2000); **92**, 508 (1990).
[17] B. Delley, Int. J. Quantum Chem. **69**, 423 (1998).
[18] H.J. Monkhorst and J.D. Pack, Phys. Rev. B **13**, 5188 (1976).
[19] G. Gilat and L.J. Raubenheimer, Phys. Rev. **144**, 390 (1966); O. Jepsen and O.K. Andersen, Solid State Commun. **9**, 1763 (1971); G. Lehmann and M. Taut, Phys. Status Solidi B **54**, 469 (1972).
[20] J.P. Perdew, K. Burke, and M. Ernzerhof, Phys. Rev. Lett. **77**, 3865 (1996).
[21] S.B. Zhang, S.H. Wei, A. Zunger, and H. Katayama-Yoshida, Phys. Rev. B **57**, 9642 (1998); S.H. Wei, S.B. Zhang, and A. Zunger, J. Appl. Phys. **85**, 7214 (1999).
[22] T. Asada and K. Terakura, Phys. Rev. B **43**, 13 599 (1993).
[23] M. Bernasconi, G.L. Chiarotti, and E. Tosatti, Phys. Rev. Lett. **70**, 3295 (1993).
[24] N. W. Ashcroft and N. D. Mermin, *Solid State Physics*, (Saunders, PA, 1976).
[25] J. L. Shay and J. H. Wernick, *Ternary Chalcopyirite Semiconductors: Growth, Electronic Properties and Applications* (Pergamon Press, Oxford, 1974).
[26] K. Sato and H. Katayama-Yoshida, Jpn. J. Appl. Phys., Part 2 **40**, L651 (2001).
[27] T.C. Schulthess and W.H. Butler, J. Appl. Phys. **89**, 7021 (2001).
[28] H. Akai, Phys. Rev. Lett. **81**, 3002 (1998).
[29] A. Twardowski, H.J.M. Swagten, and W.J.M. de Jonge, Phys. Rev. B **36**, 7013 (1987).
[30] H.T. Diep and H. Kawamura, Phys. Rev. B **40**, 7019 (1989).